Carbohydrate Polymer Technologies and Applications 2 (2021) 100075

Contents lists available at ScienceDirect

Carbohydrate Polymer Technologies and Applications

journal homepage: www.elsevier.com/locate/carpta

Xanthan-based polysaccharide/protein nanoparticles: Preparation, characterization, encapsulation and stabilization of curcumin

Aristeidis Papagiannopoulos[a,*], Aggeliki Sklapani[b]

[a] Theoretical and Physical Chemistry Institute, National Hellenic Research Foundation, 48 Vassileos Constantinou Avenue, 11635 Athens, Greece
[b] National Technical University of Athens, Physics Department, Iroon Politechneiou 9, Zografou Campus, 15780 Athens, Greece

ARTICLE INFO

Keywords:
Curcumin
Xanthan gum
Bovine serum albumin
Electrostatic complexation
Thermal treatment

ABSTRACT

This work presents the use of xanthan gum (XG) to prepare protein-containing nanoparticles (NPs). A biocompatible methodology of electrostatic complexation at acidic pH and subsequent thermal treatment is applied using the protein bovine serum albumin (BSA). The NPs have well-defined size and molar mass and are stable upon increase of pH. The secondary conformation of BSA appears irreversibly changed upon thermal treatment within the complexes with XG. The NPs inherit the properties of BSA as they are found to have hydrophobic domains and pH-dependent surface charge. XG-BSA NPs are able to bind the nutraceutical substance curcumin (CUR) and protect its structure against degradation at neutral pH. This investigation introduces the employment of XG for the formulation of protein NPs as nanocarriers of bioactive compounds.

1. Introduction

Xanthan gum (XG) is a high molar mass polysaccharide secreted by *Xanthomonas campestris* and customarily produced by fermentation (Sworn, 2009). It is an anionic polyelectrolyte with trisaccharide side-chains grafted on a backbone of cellulose (Born, Langendorff & Boulenguer, 2005). Its charge originates from the mannose groups of the side-chains which can be either pyruvate residues (terminal group) or acetylated to some degree (internal group) (Wyatt & Liberatore, 2010). In aqueous media it forms self-similar viscoelastic fluids (Papagiannopoulos, Sotiropoulos & Pispas, 2016) and it can transform into colloidal liquids upon interaction with charged substances such as cationic surfactants (Sotiropoulos & Papagiannopoulos, 2017). It is widely applied in food industry as it is an outstanding viscosity modifier and additionally can be used *quantum satis* (Born, Langendorff & Boulenguer, 2005). XG has been used in biomedical applications such as in drug delivery in combination with chitosan (Malik et al., 2020), as basis for scaffolds for cell culture (Elizalde-Peña et al., 2013) and in tissue engineering (Kumar, Rao & Han, 2018).

Protein NPs are biocompatible, biodegradable, metabolizable and nontoxic and are attractive for pharmaceutical and nutraceutical compounds delivery applications (Jain, Singh, Arya, Kundu & Kapoor, 2018; Lohcharoenkal, Wang, Chen & Rojanasakul, 2014; Verma, Gulati, Kaul, Mukherjee & Nagaich, 2018). There are several established methods to synthesize protein NPs such as desolvation (Langer, Balthasar, Vogel, Dinauer, von Briesen & Schubert, 2003), electrospraying (Wu, MacKay, McDaniel, Chilkoti & Clark, 2009) and emulsion-solvent evaporation (Yang, Cui, Cun, Tao, Shi & Lin, 2007). Electrostatic complexation with polysaccharides is a versatile technique to create protein NPs by self-assembly (Comert, Malanowski, Azarikia & Dubin, 2016) and offers biocompatibility and nontoxicity. Recently, the instability in polysaccharide/protein complexes upon pH changes has been addressed by thermal treatment elaborating on the protein-protein bridges formed upon denaturation of the complexed proteins (Jones, Decker & McClements, 2010; Jones & McClements, 2010). This way, well-defined and stimuli-responsive NPs have been developed which also have the ability to encapsulate hydrophobic bioactive substances (Papagiannopoulos & Vlassi, 2019; Vlassi & Papagiannopoulos, 2020). These NPs inherit the ability of proteins to interact with components of different nature via their hydrophobicity and charge patch. Xu et al. (2015; 2018b) have reported XG in complexes with lysozyme at pH where both biopolymers had negative net charge using alkali coupled thermal treatment and shown their promising properties as Pickering emulsions (Xu et al., 2018a).

As XG is a safe biopolymer for use in pharmaceutical and food science it is of interest to explore its potential in formation of protein-containing NPs. In this work the recently introduced methodology of thermal treatment of polysaccharide/protein electrostatic complexes into stable NPs is used for the preparation of XG-BSA NPs. This protocol includes biocompatible components and no chemical reaction or toxic solvent. The optimal solution conditions for the formation of XG-BSA complexes with high molar mass and monomodal size distribution are found by static

* Corresponding author.
E-mail address: apapagiannopoulos@eie.gr (A. Papagiannopoulos).

https://doi.org/10.1016/j.carpta.2021.100075
Received 5 January 2021; Received in revised form 5 April 2021; Accepted 8 April 2021
Available online 20 April 2021

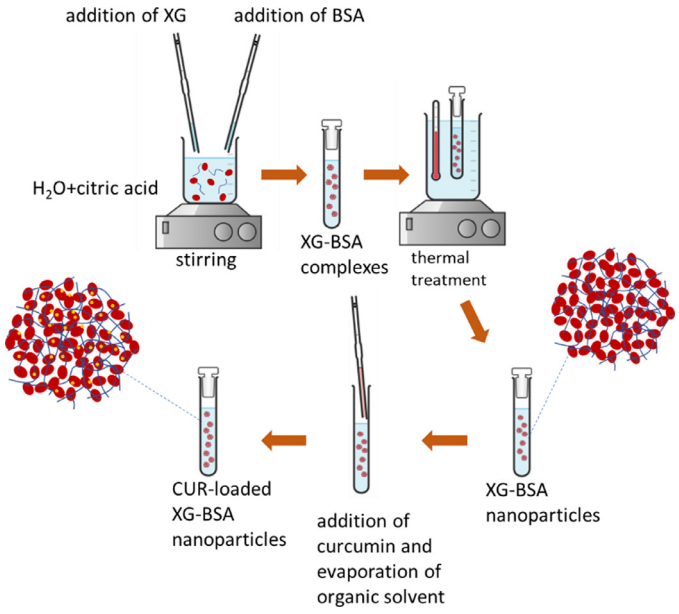

Scheme 1. Preparation route of XG-BSA NPs and loading of CUR.

and dynamic light scattering (DLS and SLS) experiments. The alterations of BSA's secondary structure upon thermal treatment and complexation are quantified by infrared spectroscopy. Surface charge and hydrophobicity properties of the produced NPs prove their potential for interaction with bioactive compounds. Finally, their ability to encapsulate and stabilize curcumin (CUR) supports their possible future use as nanocarriers of bioactive substances.

2. Materials and methods

2.1. Materials and samples preparation

Bovine serum albumin (BSA), citric acid (CA), curcumin (CUR), 8-Anilino-1-naphthalenesulfonate (ANS), pyrene, NaCl and NaOH were purchased from Sigma-Aldrich. Xanthan Gum (XG) was provided from CP Kelco. The chemical structure of XG and CUR are now provided in Scheme S1 and S2 respectively. Stock aqueous solutions of XG (1.0 $mgml^{-1}$), BSA (10 $mgml^{-1}$) and CA (1.0 $mgml^{-1}$) were prepared under stirring and kept for 20 h at 4°C to equilibrate. XG-BSA complexes were prepared by mixing proper volumes of distilled water and stock solutions under gentle stirring (Scheme 1). Firstly, CA solution was added to distilled water until pH was fixed at 5. XG solution was subsequently added and BSA solution was introduced at the end. Solutions with complexes were kept for 20 h to equilibrate at 4°C. XG-BSA NPs were prepared by applying a temperature treatment protocol on sealed vials which included heating at 70°C for 5 min under stirring and subsequent cooling at 25°C. NaOH was used to set the pH to 7. NaCl was used for experiments with salt.

For experiments on the NPs hydrophobicity 10 μl ANS dispersion 5 mM in distilled water was added to each sample solution (total volume 1 ml) and left for 20 h at 4°C to equilibrate. In the experiments with pyrene 1 μl of pyrene was added to each sample solution (total volume 1 ml) and kept for 20 h at 4°C. In order to load CUR to the prepared NPs the bioactive compound was dispersed in ethanol at 70 μM and aliquots of 5 μl from this dispersion were added to the sample solutions. The samples were left for 4–5 h without a lid under a fume cupboard for the ethanol to evaporate. All experiments were performed at 25°C and at least in triplicate while presented values are in the form of mean and standard deviation.

2.2. Light Scattering

Analysis of light scattering was conducted with an ALV system (ALV-CG-3 goniometer/ALV-5000/EPP multi tau digital correlator) and a He-Ne laser (λ = 632.8 nm). Measurements of Rayleigh ratio $R(q)$ in static light scattering (SLS) were performed to extract the weight average molecular (Chu, 1991) weight M as well as the form factor of the scattering particles $P(q)$ (equation 1).

$$\frac{Kc}{R(q)} = \frac{1}{M\ P(q)} \tag{1}$$

Where c is the mass concentration of the solute molecules, q is scattering wave vector $q = \frac{4\pi\, n_0}{\lambda} \sin\frac{\theta}{2}$. K stands for LS contrast factor $K = \frac{4\pi^2 n_0^2}{N_A \lambda^4} (\frac{\partial n}{\partial c})^2$ with n_0 being the solvent's refractive index and $\frac{\partial n}{\partial c}$ the refractive index increment of the solute system. We used $\frac{\partial n}{\partial c}$ = 0.18 mlg^{-1} for all cases. A weight average over BSA's (Jung, Choi, Kim & Moon, 2006; Khago, Bierma, Roskamp, Kozlyuk & Martin, 2018; Wang & Lucey, 2003) and XG's (Milas, Reed & Printz, 1996) $\frac{\partial n}{\partial c}$ i.e. $\frac{\partial n}{\partial c} = \frac{c_{BSA}}{c_{BSA}+c_{XG}} (\frac{\partial n}{\partial c})_{BSA} + \frac{c_{XG}}{c_{BSA}+c_{XG}} (\frac{\partial n}{\partial c})_{XG}$ with $(\frac{\partial n}{\partial c})_{BSA} = 0.185\ mlg^{-1}$ and $(\frac{\partial n}{\partial c})_{XG} = 0.155\ mlg^{-1}$ leads to a $\frac{\partial n}{\partial c}$ about 0.18 mlg^{-1} for all mass ratios used in this study.

$$\frac{R\,(q)}{Kc} = M \cdot e^{-\frac{1}{3}q^2 R_g^2 + B\cdot(q^2)^2} \tag{2}$$

In the standard Guinier approximation $P(q) = e^{-\frac{1}{3}q^2 R_g^2}$ the radius of gyration R_g of the scattering particles is extracted (Borsali & Pecora, 2008). In order for all Guinier plots to be fitted, a quadratic approximation in q^2 for the form factor (equation 2) was used (see Results and Discussion).

Dynamic light scattering (DLS) provides the scattered light intensity autocorrelation functions $g_2(\tau)$ where τ is the lag-time (Berne & Pecora, 2000). Using the Siegert relation $g_2(\tau) - 1 = \beta|g_1(\tau)|^2$ with β being a normalization constant, the field autocorrelation functions $g_1(\tau)$ is calculated. CONTIN analysis was applied for the extraction of characteristic relaxation times τ_c in $g_1(\tau)$. The τ_c distributions were transformed to distributions of hydrodynamic radii R_h using $D = 1/\tau_c q^2$ and the Stokes-Einstein relation where D is the diffusion coefficient and η the solvent viscosity (equation 3).

$$R_h = \frac{k_B T}{6\pi\eta D} \tag{3}$$

The values for Boltzmann constant and temperature, k_B = 1.38064852 × 10^{-23} JK^{-1} and T = 298 K, were used respectively.

2.3. Electrophoretic light scattering

Electrophretic light scattering data were collected with a Zetasizer Nano-ZS by Malvern Instruments Ltd. Henry equation under the Smoluchowski approximation was used for the calculation of zeta potential (ζ_P). The presented results are averages of 10 measurements made at scattering angle θ = 173°.

2.4. Fourier transform infrared spectroscopy

FTIR experiments were conducted on a Bruker Equinox 55 Fourier Transform Instrument, which included an attenuated total reflectance (ATR) diamond accessory, from SENS-IR. A drop of solutions was placed at the center of the sample holder and was dried under Nitrogen. 64 scans were carried out in the range of 500–5000 cm^{-1} at a resolution of 2 cm^{-1}.

2.5. UV-Visible Spectroscopy

UV-VIS absorption spectra were recorded with a UV-vis-NIR spectrophotometer Parkin-Elmer (Lamda 19). A 1 cm-long quartz cuvette

was used for sample placement. Measurements were performed at λ between 300 and 600 nm to obtain the absorption spectrum of CUR. Maximum intensity was located at about 425 nm.

2.6. Fluorescence Spectroscopy

A Fluorolog-3 spectrofluorometer (model FL3-21, Jobin Yvon-Spex) with a double-grating excitation and a single-grating emission was engaged. The excitation wavelength was $\lambda = 370$ nm for ANS, $\lambda = 330$ nm for pyrene, $\lambda = 290$ nm for tryptophan (TRP) and $\lambda = 420$ nm for CUR while the region of spectra recording was 390–700 nm, 350–500 nm, 310–420 nm and 440–700 nm respectively. In all measurements an integration time of 0.5 s was set.

3. Results and Discussion

3.1. Electrostatic complexation between XG and BSA

SLS and DLS were used to quantify the complexation between the two biopolymers as the combination of these methods is very sensitive in changes in molar mass of dispersed particles and their size distribution (Papagiannopoulos & Vlassi, 2019; Vlassi & Papagiannopoulos, 2020). A range of mass concentration ratios $r_m = c_{XG}/c_{BSA}$ from 10^{-3} to 10^{0} was scanned to evaluate the optimal range for the preparation of NPs. The value of pH 5 was chosen near the isoelectric point of BSA (Jachimska & Pajor, 2012; Mattison, Dubin & Brittain, 1998; Shi, Zhou & Sun, 2005; Xu, Yamanaka, Sato, Miyama & Yonese, 2000) (pI ≈ 5.4–5.5). At lower pH values e.g. pH 4–4.5 the complexation effect was very strong and not easily controllable as fibrillar macroscopic aggregates were formed in many cases.At mass concentration ratios $r_m \approx 0.1 - 0.2$ mixtures began to appear bluish due to the presence of sub-micrometer particles (200 nm) that scatter visible light strongly. At even higher r_m solutions become fairly turbid (especially after thermal treatment). Therefore, the concentration ratio range 5–8•10^{-2} was chosen as the optimal one to prepare complexes. In this range, strong interaction is observed while no macroscopic phase separation occurs.

In polyelectrolyte/protein mixtures macroscopic stoichiometric neutralization coincides with a strong increase in turbidity and signifies strong complexation (Matsunami, Kikuchi, Ogawa & Kokufuta, 2007). The mass concentration ratio where the polysaccharide charges neutralize the ones of the protein can be calculated by $\frac{c_{XG}/M_{XG}^{mon}}{c_{BSA}/M_{BSA}} = \frac{Z_{BSA}}{Z_{XG}^{mon}}$. In XG two negative charges per monomer (one disaccharide unit with a side-chain) exist therefore the net monomer charge is $Z_{XG}^{mon} = 2$. The net charge of BSA (Mattison, Dubin & Brittain, 1998) at pH 5 is $Z_{BSA} = 6.5$ The respective molar masses of XG monomer and BSA are $M_{XG}^{mon} = 934\ gmol^{-1}$ and $M_{BSA} = 66400\ gmol^{-1}$. This results to $r_m \approx 0.04 - 0.05$ which is in agreement with the optimized range in this study. At the chosen ratios there are roughly 4 to 6 XG monomers per BSA globule in solution. We have found optimal complexation in the regime of macroscopic charge neutrality in our previous works in a similar manner (Papagiannopoulos & Vlassi, 2019; Vlassi & Papagiannopoulos, 2020).

The analysis of SLS with Guinier plots (Fig. 1a) was made by a quadratic approximation (equation 2). The nonlinear trend of the plots originates from the fact that the observed radii of gyration are higher than 100 nm and therefore for values of q where $q > 1/R_g$ internal structure of the nanocomplexes is probed (Papagiannopoulos & Vlassi, 2019).

The R_h distributions (Fig. 1b) have a single and fairly well-defined population. Average hydrodynamic radius of complexes is of the order 120–200 nm. The instability of electrostatic complexes upon pH increase is illustrated in Fig. 1c. When pH increases from 5 to 7 the monomodal distribution of complexes is destroyed and becomes very broad (Fig. 1c) pointing to disintegration of complexes into aggregates of very broad distribution. At the same time the scattered intensity drops significantly (not shown).

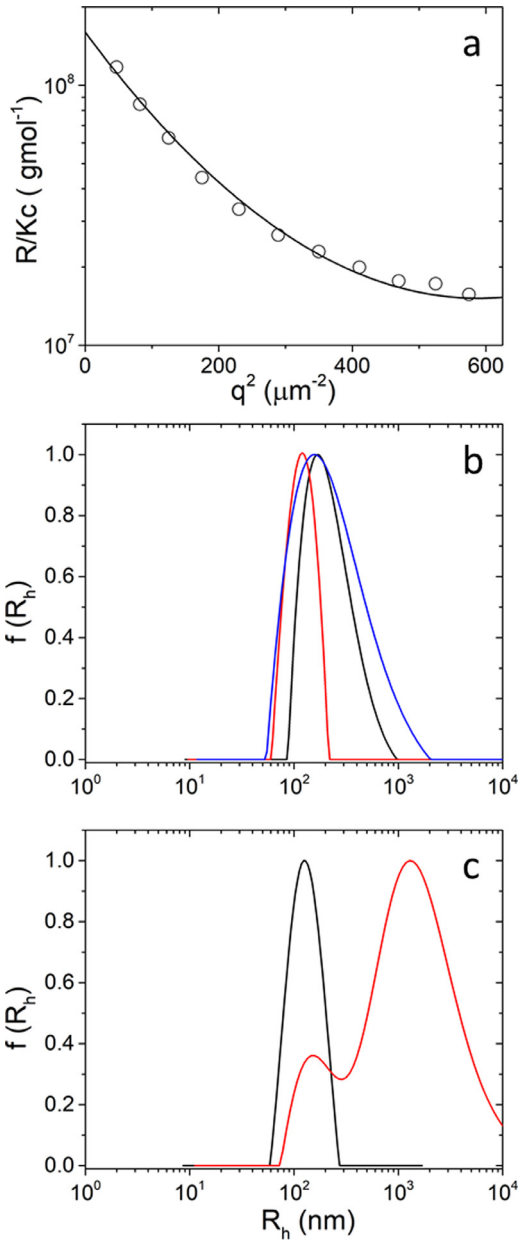

Fig. 1. (a) Guinier plot of XG-BSA complexes with r_m at 7•10^{-2} at pH 5 with 0.1 mgml^{-1} BSA. Continuous line is fitting by equation 2. (b) CONTIN analysis of XG-BSA mixtures with r_m at 5•10^{-2} (black), 6•10^{-2} (red) and 7•10^{-2} (blue) with 0.1 mgml^{-1} BSA at pH 5 (scattering angle 90°). (c) CONTIN analysis of XG-BSA mixtures with r_m at 8•10^{-2} at pH 5 (black) and pH 7 (red) and 0.1 mgml^{-1} BSA (scattering angle 90°).

3.2. Stabilization of XG-BSA NPs by thermal treatment

BSA was chosen as the protein to complex with XG because it is a model protein with well-documented thermal denaturation properties. Additionally, we have recently employed it in complexes with chondroitin sulfate (CS) and subsequent temperature-treatment stabilization (Papagiannopoulos & Vlassi, 2019). In BSA, heat induces unfolding of pockets that contain cysteine, enabling disulfide bridges between protein globules and leading to aggregation in solution (Wetzel et al., 1980). Thermal treatment at 65°C has been reported to cause partially reversible conformational changes (Takeda, Wada, Yamamoto, Moriyama & Aoki, 1989). Helicity of BSA was only partially recovered at 25°C after thermal treatment above the critical temperature

Table 1
Average parameters over the different polysaccharide/protein ratios investigated by LS.

Conditions/Parameter	M (10^8 gmol^{-1})	R_g (nm)	R_h (nm)	$\rho = R_g/R_h$
pH 5	1.5 ± 0.3	175 ± 9	156 ± 25	1.12 ± 0.19
treated pH 5	6.8 ± 2.9	170 ± 7	127 ± 7	1.33 ± 0.09
treated pH 7	6.0 ± 1.2	185 ± 20	159 ± 37	1.16 ± 0.29

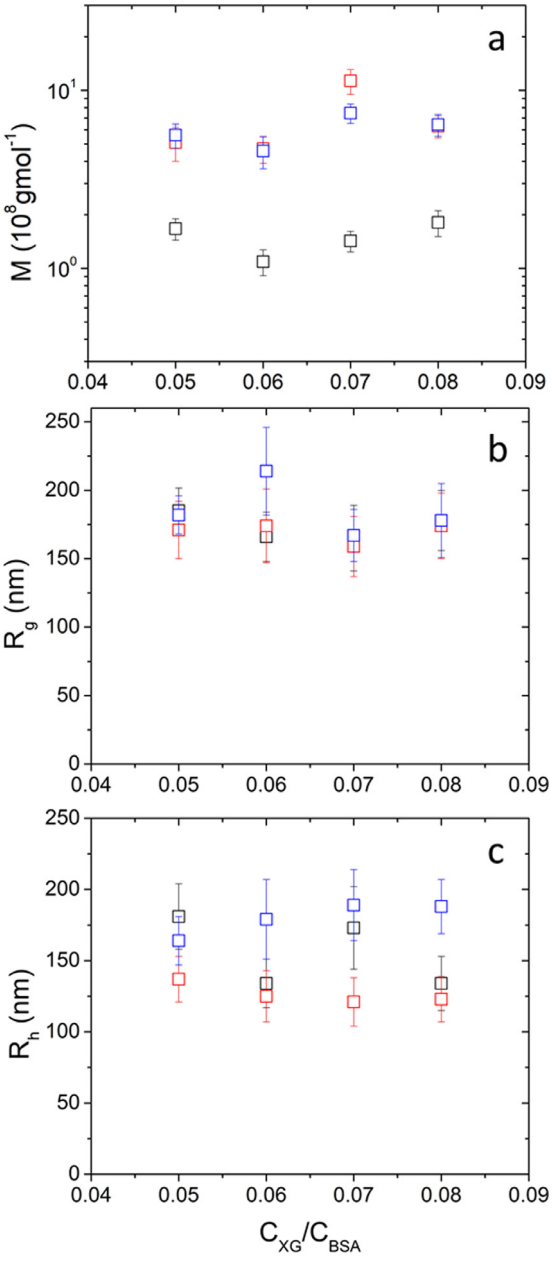

Fig. 2. (a) Apparent molar mass, (b) gyration radius and (c) hydrodynamic radius of XG-BSA complexes at pH 5 (black), NPs after thermal treatment at pH 5 (red) and thermally stabilized NPs at pH 7 (blue) with 0.1 mgml^{-1} BSA.

50°C (Moriyama, Watanabe, Kobayashi, Harano, Inui & Takeda, 2008). Detailed investigations with ATR-FTIR proposed that irreversible interglobular β-sheets form at 50–52°C and are accompanied by protein unfolding and aggregation (Lu, Li, Katzir, Raichlin, Yu & Mizaikoff, 2015).

In Figure 2a the apparent molar masses of the complexes are shown. It is evident that there is no systematic dependence as a function of XG concentration at this range of r_m. In Table 1 averages over the different mass ratios are shown. There is a strong increase in M upon thermal treatment at pH 5 which shows that denaturation of BSA's conformation possibly drives unbound globules that were free in solution to attach on the existing complexes (Papagiannopoulos & Vlassi, 2019). Setting pH to 7 BSA becomes overall negatively charged and has the same charge sign with XG. However, there is no significant change of molar mass in contrast to its dramatic drop in the case of untreated complexes. At this pH the electrostatic interactions are repulsive and the stabilizing force comes from the heat-induced interglobular connections. Additionally, XG is not inert in thermal treatment. It is a self-assembling macromolecule by forming double intermolecular helices in solution. Upon thermal treatment its native structure is renatured into a state with more double helices that enhance XG interconnections with strong effects in its morphology (Ikeda, Gohtani, Nishinari & Zhong, 2012; Matsuda, Biyajima & Sato, 2009) and mechanical properties (Oviatt & Brant, 1994; Papagiannopoulos, Sotiropoulos & Pispas, 2016). This reformation of inter-molecular double helices in XG may act synergistically with BSA thermal aggregation in stabilizing the NPs. One has to keep in mind that at low salt content ($c_S < 10^{-3}$ M) helices maybe partially destabilized and XG is in a broken helix conformation (Muller, Aurhourrache, Lecourtier & Chauveteau, 1986; Norton, Goodall, Frangou, Morris & Rees, 1984; Rochefort & Middleman, 1987). As in our case complexes are formed in the absence of salt, so that electrostatic attraction is strong, XG is expected to be in a random coil conformation with intermediate parts of helices that are susceptible to thermal effects. In any case, complexes are stabilized by heat treatment and maintain their integrity against pH changes. Consequently, thermally-treated complexes can be considered as NPs.

Radius of gyration and hydrodynamic radius are in the range 150–200 nm and they do not seem to significantly depend on the mass ratio of the two biopolymers (Figs. 2b and c). A systematic increase of R_h in the NPs upon increase in pH (Table 1) could be related to swelling due to the increase in the net electrostatic repulsions. However, this trend is not observed in R_g. In CS-BSA NPs we had clearly observed this swelling effect in SLS and DLS and confirmed it by resolving their internal correlations by small angle scattering (Papagiannopoulos, Vlassi & Radulescu, 2019). It has to be kept in mind that XG is a semi-flexible macromolecule with a persistence length 30 nm in the native single helix conformation and 125 nm in the renatured double helix conformation (Milas, Reed & Printz, 1996) and a contour length in the order of 1 μm (Papagiannopoulos, Sotiropoulos & Radulescu, 2016). The shape of the NPs can be expected to differ from spherical and LS methods are not suited to resolve shape and internal organization changes. However, the characteristic ratio R_g/R_h is about 1.1–1.3 and is compatible with the structure of randomly cross-linked microgels or mass fractal aggregates (Van Saarloos, 1987).

3.3. Protein conformation in XG-BSA NPs

FTIR experiments (Fig. 3) were performed in order to quantify the conformation of BSA in the NPs before and after thermal treatment (Figs. 3b and c). In particular, amide I band (1700–1600 cm^{-1}) was investigated as it contains information on the several structural components (Lu, Li, Katzir, Raichlin, Yu & Mizaikoff, 2015). An enhancement in absorbance is clearly observed in the region of intermolecular β-sheet (1615–1630 cm^{-1}) upon thermal treatment implying the formation of interglobular connections. Experimental data were modeled by a su-

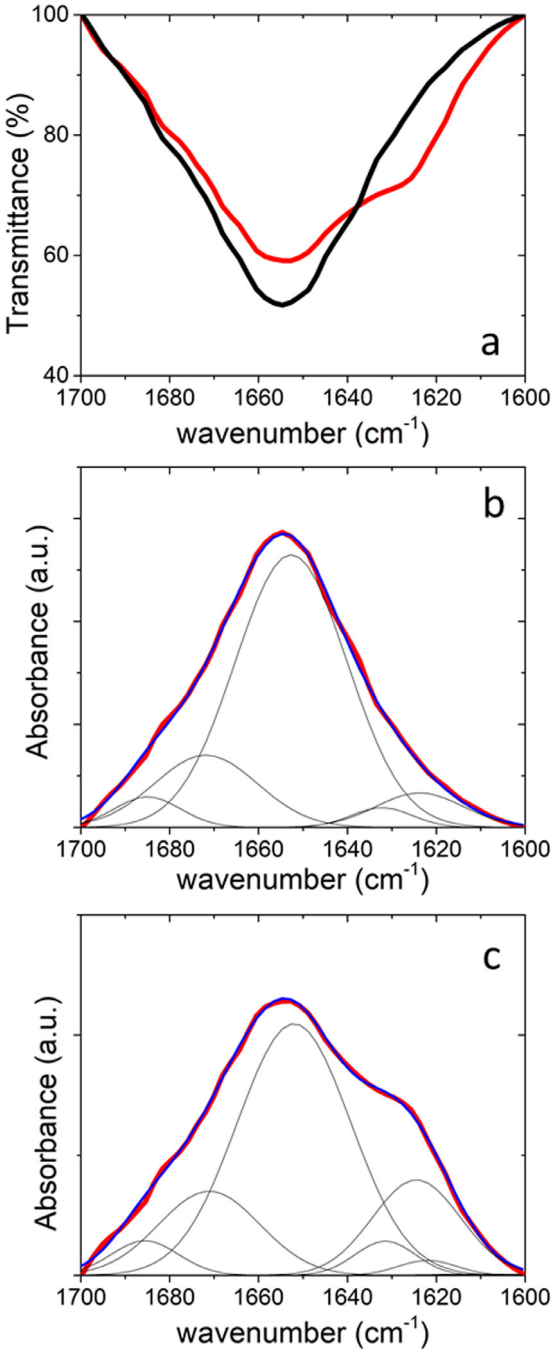

Fig. 3. (a) FTIR transmittance spectra from XG-BSA at r_m 6•10^{-2} and BSA concentration 1 mgml^{-1} at pH 5 before (black) and after (red) thermal treatment. (b and c) FTIR absorbance spectra (red) from XG-BSA at r_m 6•10^{-2} and BSA concentration 1 mgml^{-1} at pH 5 before (a) and after (b) thermal treatment. Best fits are shown in blue and separate contributions in black.

perposition of Gaussian functions (Givens, Xu, Fiegel & Grassian, 2017; Guerrero, Kerry & de la Caba, 2014; Roach, Farrar & Perry, 2005). The Gaussian peak positions were assigned to the different structural components according to table 2. The contribution from α-helix and β-sheet in the untreated BSA and XG-BSA complexes are consistent with other studies on native BSA (Murayama & Tomida, 2004; Reed, Feldhoff, Clute & Peters, 1975).

In the case of pure BSA there is no significant change after thermal treatment. Possibly treatment at 70°C for 5 min did not cause any detectable irreversible transitions. However, for complexed BSA there is a

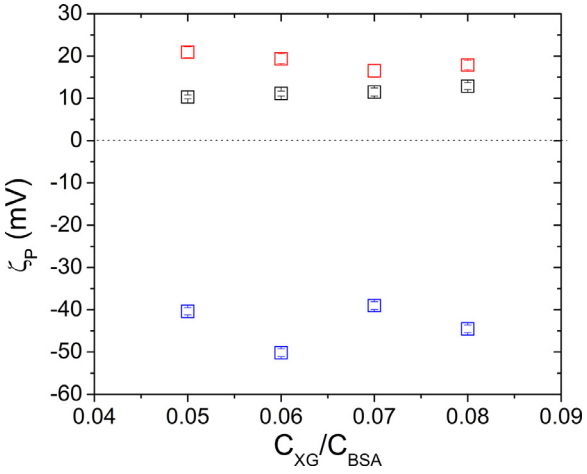

Fig. 4. Surface charge of XG-BSA complexes at pH 5 (black), NPs after thermal treatment at pH 5 (red) and thermally stabilized NPs at pH 7 (blue) at 0.1 mgml^{-1} BSA.

significant increase in intermolecular β-sheet conformation from about 8 to about 17 % (Table 2). This indicates that within the complexes with XG the protein undergoes a transition that is maintained even when temperature drops back to 25°C. Therefore, aggregation between BSA globules is possibly stabilized by the presence of the polysaccharide and a synergistic effect of the renaturation of XG double helices. The increase of intermolecular β-sheet is accompanied by a decrease in all other structural contributions. The conformational characteristics remain the same upon increase of pH to 7 showing that BSA conformation is maintained at neutral pH.

3.4. Surface charge and hydrophobicity of XG-BSA NPs

Interaction of the NPs with other biological macromolecules i.e. proteins, DNA, genes and growth factors are expected to be of electrostatic nature in many cases. The overall net surface charge of the NPs is related to their surface potential. The ζ-potential of the XG-BSA NPs before and after thermal treatment and after pH increase is shown in Fig. 4. At pH 5 ζ_P is about 11.5 mV for the complexes which is similar to what is expected from solutions of pure BSA (Jachimska & Pajor, 2012). After thermal treatment ζ_P increases to 19 mV possibly because of a preferential exposure of positively charged domains of BSA on the NP/water interface. At pH 7 ζ-potential of thermally treated NPs changes to -45 mV following the pH dependence of surface charge of BSA.

Pyrene fluorescent probe was used to investigate the existence of hydrophobic domains in the produced NPs. The I_1/I_3 ratio, between the intensities of the first (372 nm) and third (383 nm) vibronic peaks of pyrene spectrum, is traditionally used as a measure of the polarity of the microenvironment surrounding the chromophore (Dong & Winnik, 1982; Johnsson, Hansson & Edwards, 2001; Wu, Oake, Liu, Bohne & Branda, 2018). A value near 1.9 reveals a highly polar environment whereas a value near 1.0 corresponds to a nonpolar (hydrophobic environment). Pyrene has been successfully used to probe nanoenvironments in amphiphilic polymer core-shell micelles (Wang, Hou, Chen, Yan, Bai & Lu, 2016) and protein self-assemblies (Klass et al., 2019; Wu & Wang, 2017). In XG-BSA thermally stabilized NPs the I_1/I_3 ratio is about 1.4– 1.5 (Table 3) showing that environments of moderate hydrophobicity are available for the small probe to be accommodated. This is an indication that the NPs are able to encapsulate hydrophobic molecules and that they have available sites for hydrophobic interactions with other macromolecules.

Surface hydrophobicity of proteins has been customarily measured using fluorescence of ANS dye. ANS is considered to bind to nonpolar protein surfaces mainly by its hydrophobic anilinonaphthalene group.

Table 2
Secondary structure of BSA estimated from ATR-FTIR in % percentage of the separate structural components in BSA, complexes and NPs with r_m 6•10^{-2} and BSA concentration 1 mgml^{-1}.

Assignment	β-sheets and β-turns	α-helix	Short-segment chains connecting α-helical segments	Intermolecular β-sheet
Wavenumbers (cm^{-1})	1678–1688	1654–1658	1635–1639	1615–1630
BSA pH 5	19.6	71.8	1.94	6.66
BSA treated pH5	21.0	69.2	2.71	7.04
BSA treated pH 7	20.2	68.3	2.95	8.55
XG-BSA pH5	21.1	68.8	2.34	7.73
XG-BSA treated pH 5	20.2	59.1	3.23	17.5
XG-BSA treated pH 7	23.1	56.3	4.45	16.0
approx. uncertainty in estimation	1.5	3	0.5	1.6

Table 3
Results from pyrene fluorescence experiments and surface hydrophobicity (SH) on XG-BSA NPs (thermally treated).

Parameter/Sample	$r_m = 6•10^{-2}$ pH 5	pH 7	$r_m = 8•10^{-2}$ pH 5	pH 7
I_1/I_3	1.43 ± 0.05	1.46 ± 0.04	1.47 ± 0.06	1.47 ± 0.03
S_0 (10^6 CPSmg^{-1}ml)	16.0 ± 2.4	15.8 ± 3.7	14.7 ± 2.5	18.2 ± 1.0

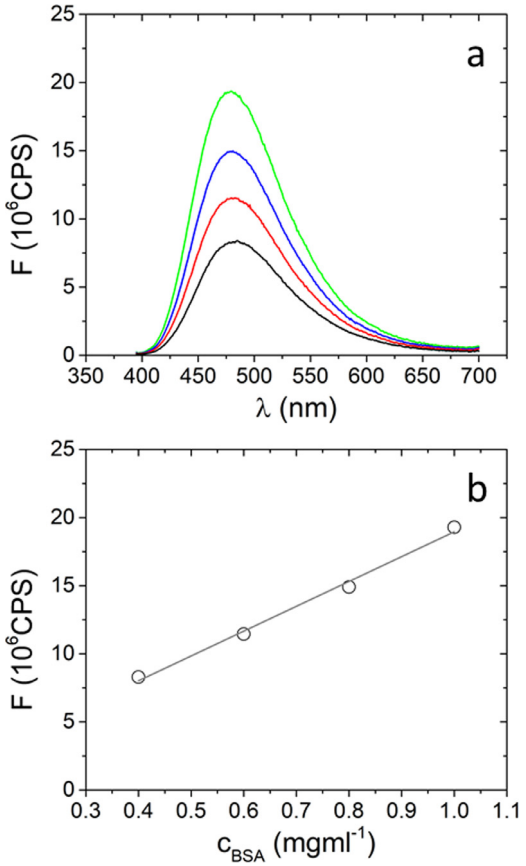

Fig. 5. (a) ANS fluorescence from thermally treated XG-BSA NPS at $r_m = 8 \cdot 10^{-2}$ at pH 7 for 0.4 (black), 0.6 (red), 0.8 (blue) and 1.0 (green) and (b) fluorescence intensity at maximum.

Binding to hydrophobic pockets causes its fluorescence to increase significantly to levels similar to the ones of ANS in organic solvents (Matulis, Baumann, Bloomfield & Lovrien, 1999). Fluorescence emission from ANS increases as more XG-BSA NPs exist in solution (Fig. 5a) showing that the NPs can encapsulate bulky hydrophobic molecules on their surface as they contain BSA. Fluorescence of ANS in blank solution was negligible (not shown).

In more detail, the maximum fluorescence intensity F shows a linear dependence on NP concentration (Fig. 5b). A measure of surface hydrophobicity (S_0) can be extracted from the slope of the F vs c_{BSA} plot by $S_0 = \frac{\Delta F}{\Delta c_{BSA}}$ and it can be used to compare between different samples (Dorh et al., 2015). The surface hydrophobicity of the NPs is apparently not affected by solution pH and therefore it can be considered that hydrophobic interactions with other molecular compounds act independently of the electrostatic ones (Table 3).

3.5. Encapsulation and stabilization of CUR in XG-BSA NPs

Curcumin has anticancer activity, it is beneficial for cardiovascular, diabetic and Alzheimer's diseases (Araújo & Leon, 2001; Goel, Kunnumakkara & Aggarwal, 2008; Kroll, 2006) and is also used in food technology and food supplement products (Kharat, Du, Zhang & McClements, 2017). It is a hydrophobic substance and consequently it has the serious drawback of extremely low solubility in water and poor bioavailability. For this reason there have been attempts towards is nanodelivery using polymer NPS, lipid NPs and other amphiphilic nanostructured materials (Sahu, Kasoju & Bora, 2008). Therefore, it is of interest to investigate the ability of the XG-BSA NPs to encapsulate and maintain CUR.

The fluorescence spectra from tryptophan residues of BSA is shown in Fig. 6a. The effect of quenching is illustrated by the intensity drop. As concentration of CUR increases more molecules interact with tryptophan residues by hydrophobic interaction. The fluorescence intensity at maximum F maybe used to further characterize the binding process. In the Stern-Volmer equation (Mohammadi, Bordbar, Divsalar, Mohammadi & Saboury, 2009) a quenching constant K_{SV} is extracted from $\frac{F_0-F}{F} = K_{SV} \cdot c_{CUR}$ where F_0 is the intensity in the absence of CUR (Figure 6a, insert). In another representation (Barik, Priyadarsini & Mohan, 2003; Mohammadi, Bordbar, Divsalar, Mohammadi & Saboury, 2009) the binding constant K_A can be estimated by $ln(\frac{F_0-F}{F}) = lnK_A + n \cdot lnc_{CUR}$ where n is the number of binding sites per protein globule. The estimated constants $K_{SV} \approx 1.3 \cdot 10^6 M^{-1}$ and $K_A \approx 0.9 \cdot 10^6 M^{-1}$ and $n \approx 1.3$ (Table 4) are consistent with previous studies on CUR binding on pure BSA (Barik, Priyadarsini & Mohan, 2003; Mohammadi, Bordbar,

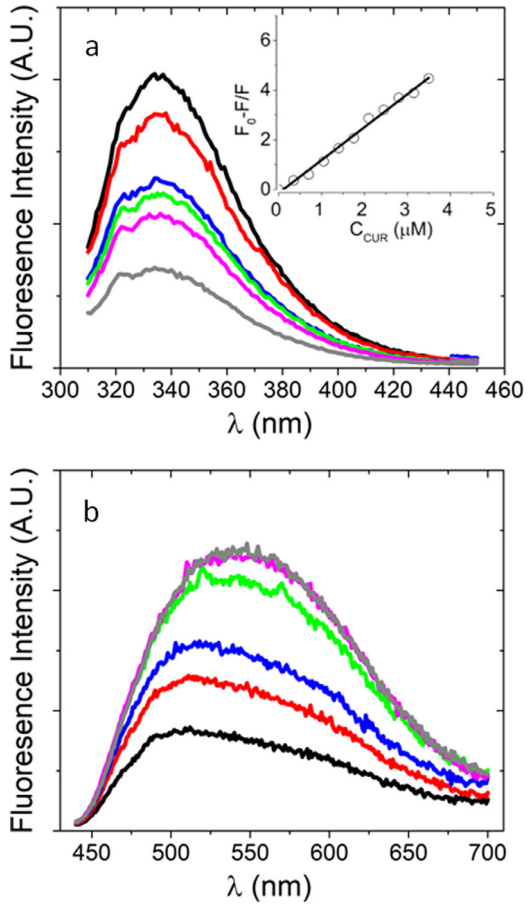

Fig. 6. (a) Tryptophan fluorescence from thermally treated XG-BSA NPS at r_m = $8 \cdot 10^{-2}$ and pH 7 for 1.0 mgml^{-1} BSA at 0 (black), 0.35 (red), 0.70 (blue), 1.05 (green), 1.40 (magenta) and 1.75 (gray) μM CUR. Insert: fluorescence intensity at maximum. (b) CUR fluorescence from thermally treated XG-BSA NPS at r_m = $6 \cdot 10^{-2}$ and pH 7 for 1.0 mgml^{-1} BSA with the same color assignments as in (a).

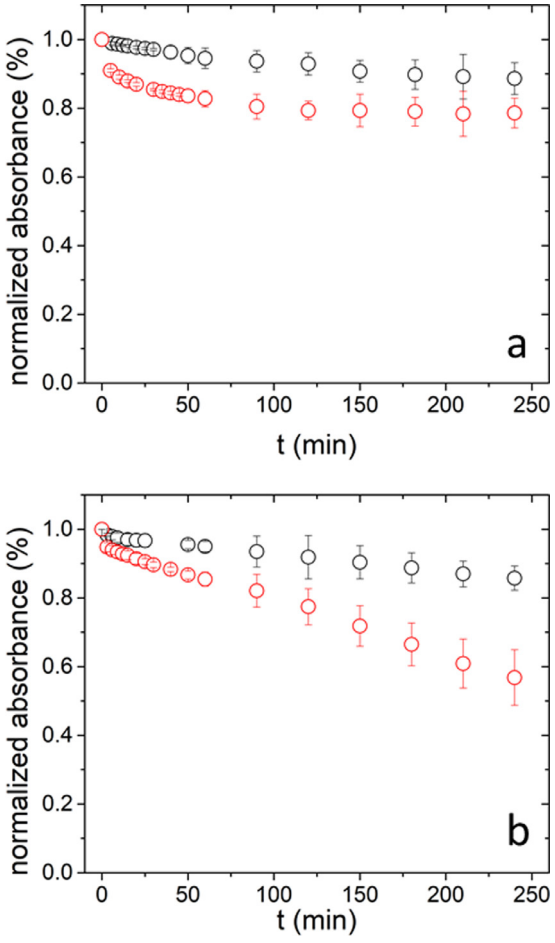

Fig. 7. Absorbance of CUR at 425 nm in the presence (black) and absence (red) of thermally treated XG-BSA NPs at $r_m = 7 \cdot 10^{-2}$ and 1.0 mgml^{-1} BSA at pH 5 (a) and pH 7 (b).

Table 4
Stern-Volmer constant K_{SV}, binding constant K_A and number of binding sites n from tryptophan fluorescence and binding constant K_B from CUR fluorescence of XG-BSA NPs (thermally treated) at pH 7.

Parameter/sample	$r_m = 6 \bullet 10^{-2}$	$r_m = 8 \bullet 10^{-2}$
$K_{SV}(10^6 M^{-1})$	1.32 ± 0.05	1.29 ± 0.07
$K_A(10^6 M^{-1})$	0.96 ± 0.12	0.76 ± 0.10
n	1.18 ± 0.13	1.43 ± 0.09
$K_B(10^6 M^{-1})$	0.10 ± 0.24	0.078 ± 0.013

Divsalar, Mohammadi & Saboury, 2009) showing that the NPs inherit BSA's ability to encapsulate CUR.

Binding of CUR to BSA can be also demonstrated by measuring the emission of the curcuminoid itself. CUR's fluorescence is negligible in the absence of BSA. CUR molecules bound to BSA emit fluorescence radiation (Fig. 6b). One can use $\frac{1}{\Delta F} = \frac{1}{\Delta F_{max}} \cdot (1 + \frac{1}{K_B \cdot c_{CUR}})$ where ΔF is the difference between measured and maximum intensity (saturation) and ΔF_{max} the saturation intensity (Sahu, Kasoju & Bora, 2008) to obtain a binding constant K_B. The value of K_B is an order of magnitude lower than the other two binding constants (Table 4). This kind of difference has been also observed in CUR binding to casein micelles (Sahu, Kasoju & Bora, 2008).

CUR's stability is very important so that its physiological activities are maintained (Lee, Loo, Bebawy, Luk, Mason & Rohanizadeh, 2013; Wang et al., 1997) . In solutions CUR degrades slowly while in neutral and basic pH it degrades more rapidly because of proton removal from the phenolic group which causes a compromise in its conjugated diene structure (Wang et al., 1997). CUR is stabilized by proteins (Mirzaee et al., 2019), protein NPs (Wu & Wang, 2017) and polysaccharide NPs (Boruah, Saikia & Dutta, 2012) in aqueous media of neutral pH. An amount of residual CUR of about 80% has been observed in BSA solutions after 5 h of incubation (Mirzaee et al., 2019) at pH 7.

Degradation kinetics of CUR in aqueous media can be investigated by monitoring its absorbance at maximum (425 nm) as a function of time (Mondal, Ghosh & Moulik, 2016; Wu & Wang, 2017). At pH 5 CUR absorbance is fairly stable either the XG-BSA NPs are present or not (Fig. 7a). In more detail, about 90 % of absorbance remains in the presence of NPs and 80 % in their absence after 250 min. At pH 7 NPs preserve more than 85 % of CUR absorbance whereas in blank solutions absorbance drops to lower than 60 %. The produced NPs are able to sustain CUR solubilized in solution and keep it from degradation.

3.6. Stability of blank and CUR-loaded XG-BSA NPs in salt solutions

In order to test the colloidal stability of the NPs in salt concentrations that simulate physiological conditions, experiments were performed in pure NPs and NPs loaded with CUR. It was found that molar mass, gyration radius and hydrodynamic radius did not significantly change as a function of salt content or by the presence of CUR at pH5 and pH 7 (Figure S1). Only in the case of pH 5 an increase in molar mass upon addition of CUR is observed and possibly relates to the increase of hydrophobic interactions between the NPs. Apparently, the moderate ζ-potential (~ +20 mV) of the NPs does not totally prevent inter-particle aggregation.

However, at pH 7 where ζ-potential is comparably high (~ -45 mV) molar mass remains unaffected by the presence of CUR indicating that aggregation at pH 5 is weak and reversible. These observations support further the possibilities of the produced NPs as candidates for nanodelivery in relevant medical and food science applications. It has to be noted that NPs with or without loaded CUR were stable for at least one week after their preparation.

4. Conclusions

We applied a thermal treatment protocol to stabilize XG-BSA electrostatic complexes into stable NPs. The size and molar mass of complexes and NPs and the effect of pH is characterized by SLS and DLS. The produced NPs are stable contrary to the untreated complexes while BSA's conformation is irreversibly changed within the complexes upon thermal treatment. The NPs are tested in regard to their surface charge and surface hydrophobicity. ζ-Potential is pH-tunable whereas its ability to bind the hydrophobic substances ANS and pyrene is pH-independent. Encapsulation of CUR from the NPs is investigated in detail, binding characteristics are consistent with the ones of CUR to pure BSA and NPs are found capable of preserving CUR's functional structure at pH 7. This work motivates the use of XG in polysaccharide-protein NPs for the encapsulation of pharmaceutical and nutrition compounds for possible delivery applications in biomedicine and food science.

Declaration of Competing Interest

The authors declare no conflict of interest.

Supplementary materials

Supplementary material associated with this article can be found, in the online version, at doi:10.1016/j.carpta.2021.100075.

References

Araújo, C. C., & Leon, L. L. (2001). Biological activities of Curcuma longa L. *Memorias Do Instituto Oswaldo Cruz, 96*(5), 723–728.

Barik, A., Priyadarsini, K. I., & Mohan, H. (2003). Photophysical studies on binding of curcumin to bovine serum albumin¶. *Photochemistry and Photobiology, 77*(6), 597–603.

Berne, B. J., & Pecora, R. (2000). *Dynamic Light Scattering, With Applications to Chemistry, Biology, and Physics*. Toronto: Dover.

Born, K., Langendorff, V., & Boulenguer, P. (2005). Xanthan. *Biopolymers Online*. Wiley-VCH Verlag GmbH & Co. KGaA.

Borsali, R., & Pecora, R. (2008). *Soft-Matter Characterization*. Springer.

Boruah, B., Saikia, P. M., & Dutta, R. K. (2012). Binding and stabilization of curcumin by mixed chitosan–surfactant systems: a spectroscopic study. *Journal of Photochemistry and Photobiology A: Chemistry, 245*, 18–27.

Chu, B. (1991). *Laser Light Scattering*. New York: Academic Press.

Comert, F., Malanowski, A. J., Azarikia, F., & Dubin, P. L. (2016). Coacervation and precipitation in polysaccharide-protein systems. *Soft Matter, 12*(18), 4154–4161.

Dong, D. C., & Winnik, M. A. (1982). The Py scale of solvent polarities. solvent effects on the vibronic fine structure of pyrene fluorescence and empirical correlations with ET and Y values. *Photochemistry and Photobiology, 35*(1), 17–21.

Dorh, N., Zhu, S., Dhungana, K. B., Pati, R., Luo, F.-T., Liu, H., & Tiwari, A. (2015). BODIPY-based fluorescent probes for sensing protein surface-hydrophobicity. *Scientific Reports, 5*(1), 18337.

Elizalde-Peña, E. A., Zarate-Triviño, D. G., Nuño-Donlucas, S. M., Medina-Torres, L., Gough, J. E., Sanchez, I. C., Villaseñor, F., & Luna-Barcenas, G. (2013). Synthesis and characterization of a hybrid (chitosan-g-glycidyl methacrylate)–xanthan hydrogel. *Journal of Biomaterials Science, Polymer Edition, 24*(12), 1426–1442.

Givens, B. E., Xu, Z., Fiegel, J., & Grassian, V. H. (2017). Bovine serum albumin adsorption on SiO2 and TiO2 nanoparticle surfaces at circumneutral and acidic pH: A tale of two nano-bio surface interactions. *Journal of Colloid and Interface Science, 493*, 334–341.

Goel, A., Kunnumakkara, A. B., & Aggarwal, B. B. (2008). Curcumin as "Curecumin": From kitchen to clinic. *Biochemical Pharmacology, 75*(4), 787–809.

Guerrero, P., Kerry, J. P., & de la Caba, K. (2014). FTIR characterization of protein–polysaccharide interactions in extruded blends. *Carbohydrate Polymers, 111*, 598–605.

Ikeda, S., Gohtani, S., Nishinari, K., & Zhong, Q. (2012). Single molecules and networks of Xanthan Gum Probed by atomic force microscopy. *Food Sci Technol Res, 18*(5), 741–745.

Jachimska, B., & Pajor, A. (2012). Physico-chemical characterization of bovine serum albumin in solution and as deposited on surfaces. *Bioelectrochemistry, 87*, 138–146.

Jain, A., Singh, S. K., Arya, S. K., Kundu, S. C., & Kapoor, S. (2018). Protein nanoparticles: promising platforms for drug delivery applications. *ACS Biomaterials Science & Engineering, 4*(12), 3939–3961.

Johnsson, M., Hansson, P., & Edwards, K. (2001). Spherical micelles and other self-assembled structures in dilute aqueous mixtures of Poly(Ethylene Glycol) Lipids. *The Journal of Physical Chemistry B, 105*(35), 8420–8430.

Jones, O. G., Decker, E. A., & McClements, D. J. (2010). Comparison of protein–polysaccharide nanoparticle fabrication methods: Impact of biopolymer complexation before or after particle formation. *Journal of Colloid and Interface Science, 344*(1), 21–29.

Jones, O. G., & McClements, D. J. (2010). Biopolymer nanoparticles from heat-treated electrostatic protein–polysaccharide complexes: factors affecting particle characteristics. *Journal of Food Science, 75*(2), N36–N43.

Jung, S. H., Choi, S. J., Kim, H. J., & Moon, T. W. (2006). Molecular characteristics of bovine serum albumin-dextran conjugates. *Bioscience, Biotechnology, and Biochemistry, 70*(9), 2064–2070.

Khago, D., Bierma, J. C., Roskamp, K. W., Kozlyuk, N., & Martin, R. W. (2018). Protein refractive index increment is determined by conformation as well as composition. *Journal of Physics: Condensed Matter, 30*, Article 435101.

Kharat, M., Du, Z., Zhang, G., & McClements, D. J. (2017). Physical and chemical stability of curcumin in aqueous solutions and emulsions: impact of ph, temperature, and molecular environment. *Journal of Agricultural and Food Chemistry, 65*(8), 1525–1532.

Klass, S. H., Smith, M. J., Fiala, T. A., Lee, J. P., Omole, A. O., Han, B.-G., Downing, K. H., Kumar, S., & Francis, M. B. (2019). Self-assembling micelles based on an intrinsically disordered protein domain. *Journal of the American Chemical Society, 141*(10), 4291–4299.

Kroll, D. J. (2006). Phytopharmaceuticals in Cancer Chemoprevention Edited by D. Bagchi (Creighton University) and H. G. Preuss (Georgetown University). CRC Press, Boca Raton. 2005. xvi + 665 pp. 18 × 26 cm. $139.95. ISBN 0-8493-1560-3. *Journal of Natural Products, 69*(2), 308–309.

Kumar, A., Rao, K. M., & Han, S. S. (2018). Application of xanthan gum as polysaccharide in tissue engineering: A review. *Carbohydrate Polymers, 180*, 128–144.

Langer, K., Balthasar, S., Vogel, V., Dinauer, N., von Briesen, H., & Schubert, D. (2003). Optimization of the preparation process for human serum albumin (HSA) nanoparticles. *International Journal of Pharmaceutics, 257*(1), 169–180.

Lee, W.-H., Loo, C.-Y., Bebawy, M., Luk, F., Mason, R. S., & Rohanizadeh, R. (2013). Curcumin and its derivatives: their application in neuropharmacology and neuroscience in the 21st century. *Current neuropharmacology, 11*(4), 338–378.

Lohcharoenkal, W., Wang, L., Chen, Y. C., & Rojanasakul, Y. (2014). Protein nanoparticles as drug delivery carriers for cancer therapy. *BioMed Research International, 2014*, Article 180549.

Lu, R., Li, W.-W., Katzir, A., Raichlin, Y., Yu, H.-Q., & Mizaikoff, B. (2015). Probing the secondary structure of bovine serum albumin during heat-induced denaturation using mid-infrared fiberoptic sensors. *Analyst, 140*(3), 765–770.

Malik, N. S., Ahmad, M., Minhas, M. U., Tulain, R., Barkat, K., Khalid, I., & Khalid, Q. (2020). Chitosan/Xanthan gum based hydrogels as potential carrier for an antiviral drug: fabrication, characterization, and safety evaluation. *Frontiers in chemistry, 8* 50-50.

Matsuda, Y., Biyajima, Y., & Sato, T. (2009). Thermal denaturation, renaturation, and aggregation of a double-helical polysaccharide Xanthan in aqueous solution. *Polym. J, 41*(7), 526–532.

Matsunami, H., Kikuchi, R., Ogawa, K., & Kokufuta, E. (2007). Light scattering study of complex formation between protein and polyelectrolyte at various ionic strengths. *Colloids and Surfaces B: Biointerfaces, 56*(1), 142–148.

Mattison, K. W., Dubin, P. L., & Brittain, I. J. (1998). Complex formation between bovine serum albumin and strong polyelectrolytes: effect of polymer charge density. *The Journal of Physical Chemistry B, 102*(19), 3830–3836.

Matulis, D., Baumann, C. G., Bloomfield, V. A., & Lovrien, R. E. (1999). 1-Anilino-8-naphthalene sulfonate as a protein conformational tightening agent. *Biopolymers, 49*(6), 451–458.

Milas, M., Reed, W. F., & Printz, S. (1996). Conformations and flexibility of native and re-natured xanthan in aqueous solutions. *International Journal of Biological Macromolecules, 18*(3), 211–221.

Mirzaee, F., Hosseinzadeh, L., Ashrafi-Kooshk, M. R., Esmaeili, S., Ghobadi, S., Farzaei, M. H., Zad-Bari, M. R., & Khodarahmi, R. (2019). Diverse effects of different "Protein-Based" vehicles on the stability and bioavailability of curcumin: spectroscopic evaluation of the antioxidant activity and Cytotoxicity In Vitro. *Protein and Peptide Letters, 26*(2), 132–147.

Mohammadi, F., Bordbar, A.-K., Divsalar, A., Mohammadi, K., & Saboury, A. A. (2009). Analysis of binding interaction of curcumin and diacetylcurcumin with human and bovine serum albumin using fluorescence and circular dichroism spectroscopy. *The Protein Journal, 28*(3), 189–196.

Mondal, S., Ghosh, S., & Moulik, S. P. (2016). Stability of curcumin in different solvent and solution media: UV–visible and steady-state fluorescence spectral study. *Journal of Photochemistry and Photobiology B: Biology, 158*, 212–218.

Moriyama, Y., Watanabe, E., Kobayashi, K., Harano, H., Inui, E., & Takeda, K. (2008). Secondary structural change of bovine serum albumin in thermal denaturation up to 130°C and Protective Effect of Sodium Dodecyl Sulfate on the Change. *The Journal of Physical Chemistry B, 112*(51), 16585–16589.

Muller, G., Aurhourrache, M., Lecourtier, J., & Chauveteau, G. (1986). Salt dependence of the conformation of a single-stranded xanthan. *International Journal of Biological Macromolecules, 8*(3), 167–172.

Murayama, K., & Tomida, M. (2004). Heat-induced secondary structure and conformation change of bovine serum albumin investigated by fourier transform infrared spectroscopy. *Biochemistry, 43*(36), 11526–11532.

Norton, I. T., Goodall, D. M., Frangou, S. A., Morris, E. R., & Rees, D. A. (1984). Mechanism and dynamics of conformational ordering in xanthan polysaccharide. *Journal of Molecular Biology, 175*(3), 371–394.

Oviatt, H. W. J., & Brant, D. A (1994). Viscoelastic behavior of thermally treated Aqueous Xanthan solutions in the semidilute concentration regime. *Macromolecules, 27*, 2402.
Papagiannopoulos, A., Sotiropoulos, K., & Pispas, S. (2016). Particle tracking microrheology of the power-law viscoelasticity of xanthan solutions. *Food Hydrocolloids, 61*, 201–210.
Papagiannopoulos, A., Sotiropoulos, K., & Radulescu, A. (2016). Scattering investigation of multiscale organization in aqueous solutions of native xanthan. *Carbohydrate Polymers, 153*, 196–202.
Papagiannopoulos, A., & Vlassi, E. (2019). Stimuli-responsive nanoparticles by thermal treatment of bovine serum albumin inside its complexes with chondroitin sulfate. *Food Hydrocolloids, 87*, 602–610.
Papagiannopoulos, A., Vlassi, E., & Radulescu, A. (2019). Reorganizations inside thermally stabilized protein/polysaccharide nanocarriers investigated by small angle neutron scattering. *Carbohydrate Polymers, 218*, 218–225.
Reed, R. G., Feldhoff, R. C., Clute, O. L., & Peters, T. (1975). Fragments of bovine serum albumin produced by limited proteolysis. conformation and ligand binding. *Biochemistry, 14*(21), 4578–4583.
Roach, P., Farrar, D., & Perry, C. C. (2005). Interpretation of protein adsorption: surface-induced conformational changes. *Journal of the American Chemical Society, 127*(22), 8168–8173.
Rochefort, W. E., & Middleman, S. (1987). Rheology of Xanthan gum: salt, temperature, and strain effects in oscillatory and steady shear experiments. *Journal of Rheology, 31*(4), 337–369.
Sahu, A., Kasoju, N., & Bora, U. (2008). Fluorescence study of the curcumin-casein micelle complexation and its application as a drug nanocarrier to cancer cells. *Biomacromolecules, 9*(10), 2905–2912.
Shi, Q., Zhou, Y., & Sun, Y. (2005). Influence of pH and ionic strength on the steric mass-action model parameters around the isoelectric point of protein. *Biotechnology Progress, 21*(2), 516–523.
Sotiropoulos, K., & Papagiannopoulos, A. (2017). Modification of xanthan solution properties by the cationic surfactant DTMAB. *International Journal of Biological Macromolecules, 105*, 1213–1219.
Sworn, G. (2009). Xanthan Gum. In *Food Stabilisers, Thickeners and Gelling Agents* (pp. 325–342). Wiley-Blackwell.
Takeda, K., Wada, A., Yamamoto, K., Moriyama, Y., & Aoki, K. (1989). Conformational change of bovine serum albumin by heat treatment. *Journal of Protein Chemistry, 8*(5), 653–659.
Van Saarloos, W. (1987). On the hydrodynamic radius of fractal aggregates. *Physica A: Statistical Mechanics and its Applications, 147*(1), 280–296.
Verma, D., Gulati, N., Kaul, S., Mukherjee, S., & Nagaich, U. (2018). Protein Based Nanostructures for Drug Delivery. *Journal of pharmaceutics, 2018*, Article 9285854–9285854.
Vlassi, E., & Papagiannopoulos, A. (2020). Nanoformulation of fibrinogen by thermal stabilization of its electrostatic complexes with hyaluronic acid. *International Journal of Biological Macromolecules, 158*, 251–257.
Wang, G., Hou, H., Chen, Y., Yan, C., Bai, G., & Lu, Y. (2016). Exploration of interactions between decyl-β-d-glucopyranoside and bovine serum albumin in aqueous solution. *RSC Advances, 6*(24), 19700–19706.
Wang, T., & Lucey, J. A. (2003). Use of Multi-Angle Laser Light Scattering and Size-Exclusion Chromatography to Characterize the Molecular Weight and Types of Aggregates Present in Commercial Whey Protein Products. *Journal of Dairy Science, 86*(10), 3090–3101.
Wang, Y.-J., Pan, M.-H., Cheng, A.-L., Lin, L.-I., Ho, Y.-S., Hsieh, C.-Y., & Lin, J.-K. (1997). Stability of curcumin in buffer solutions and characterization of its degradation products. *Journal of Pharmaceutical and Biomedical Analysis, 15*(12), 1867–1876.
Wetzel, R., Becker, M., Behlke, J., Billwitz, H., Böhm, S., Ebert, B., Hamann, H., Krumbiegel, J., & Lassmann, G. (1980). Temperature behaviour of human serum albumin. *European Journal of Biochemistry, 104*(2), 469–478.
Wu, T., Oake, J., Liu, Z., Bohne, C., & Branda, N. R. (2018). Probing the microenvironments in a polymer-wrapped core-shell nanoassembly using Pyrene Chromophores. *ACS omega, 3*(7), 7673–7680.
Wu, Y., MacKay, J. A., McDaniel, J. R., Chilkoti, A., & Clark, R. L. (2009). Fabrication of Elastin-Like Polypeptide Nanoparticles for Drug Delivery by Electrospraying. *Biomacromolecules, 10*(1), 19–24.
Wu, Y., & Wang, X. (2017). Binding, stability, and antioxidant activity of curcumin with self-assembled casein–dextran conjugate micelles. *International Journal of Food Properties, 20*(12), 3295–3307.
Wyatt, N. B., & Liberatore, M. W. (2010). The effect of counterion size and valency on the increase in viscosity in polyelectrolyte solutions. *Soft Matter, 6*(14), 3346–3352.
Xu, S., Yamanaka, J., Sato, S., Miyama, I., & Yonese, M. (2000). Characteristics of Complexes Composed of Sodium Hyaluronate and Bovine Serum Albumin. *Chemical & Pharmaceutical Bulletin, 48*(6), 779–783.
Xu, W., Jin, W., Huang, K., Huang, L., Lou, Y., Li, J., Liu, X., & Li, B. (2018a). Interfacial and emulsion stabilized behavior of lysozyme/xanthan gum nanoparticles. *International Journal of Biological Macromolecules, 117*, 280–286.
Xu, W., Jin, W., Li, Z., Liang, H., Wang, Y., Shah, B. R., Li, Y., & Li, B. (2015). Synthesis and characterization of nanoparticles based on negatively charged xanthan gum and lysozyme. *Food Research International, 71*, 83–90.
Xu, W., Li, B., Li, J., Huang, L., Liu, H., Zhu, D., Liu, M., & Liu, X. (2018b). Rheological and spectral analysis of xanthan gum/lysozyme system during nanoparticle fabrication. *International Journal of Food Science & Technology, 53*(11), 2595–2601.
Yang, L., Cui, F., Cun, D., Tao, A., Shi, K., & Lin, W. (2007). Preparation, characterization and biodistribution of the lactone form of 10-hydroxycamptothecin (HCPT)-loaded bovine serum albumin (BSA) nanoparticles. *International Journal of Pharmaceutics, 340*(1), 163–172.